Diagnostic PET Imaging of Mammary Microcalcifications Using ^{64}Cu-DOTA-Alendronate in a Rat Model of Breast Cancer

Bradley J. Ahrens[1–3], Lin Li[1], Alexandra K. Ciminera[3,4], Junie Chea[1], Erasmus Poku[1], James R. Bading[5], Michael R. Weist[1,3], Marcia M. Miller[6], David M. Colcher[1], and John E. Shively[1]

[1]Deparment of Molecular Immunology, Beckman Research Institute of the City of Hope, Duarte, California; [2]Division of Comparative Medicine, Beckman Research Institute of the City of Hope, Duarte, California; [3]Irell and Manella Graduate School of Biological Sciences, City of Hope, Duarte, California; [4]Department of Molecular Medicine, Beckman Research Institute of the City of Hope, Duarte, California; [5]Department of Medical Oncology, City of Hope, Duarte, California; and [6]Department of Cell and Molecular Biology, Beckman Research Institute of the City of Hope, Duarte, California

The development of improved breast cancer screening methods is hindered by a lack of cancer-specific imaging agents and effective small-animal models to test them. The purpose of this study was to evaluate ^{64}Cu-DOTA-alendronate as a mammary microcalcification-targeting PET imaging agent, using an ideal rat model. Our long-term goal is to develop ^{64}Cu-DOTA-alendronate for the detection and noninvasive differentiation of malignant versus benign breast tumors with PET. **Methods:** DOTA-alendronate was synthesized, radiolabeled with ^{64}Cu, and administered to normal or tumor-bearing aged, female, retired breeder Sprague–Dawley rats for PET imaging. Mammary tissues were subsequently labeled and imaged with light, confocal, and electron microscopy to verify microcalcification targeting specificity of DOTA-alendronate and elucidate the histologic and ultrastructural characteristics of the microcalcifications in different mammary tumor types. Tumor uptake, biodistribution, and dosimetry studies were performed to evaluate the efficacy and safety of ^{64}Cu-DOTA-alendronate. **Results:** ^{64}Cu-DOTA-alendronate was radiolabeled with a 98% yield. PET imaging using aged, female, retired breeder rats showed specific binding of ^{64}Cu-DOTA-alendronate in mammary glands and mammary tumors. The highest uptake of ^{64}Cu-DOTA-alendronate was in malignant tumors and the lowest uptake in benign tumors and normal mammary tissue. Confocal analysis with carboxyfluorescein-alendronate confirmed the microcalcification binding specificity of alendronate derivatives. Biodistribution studies revealed tissue alendronate concentrations peaking within the first hour, then decreasing over the next 48 h. Our dosimetric analysis demonstrated a ^{64}Cu effective dose within the acceptable range for clinical PET imaging agents and the potential for translation into human patients. **Conclusion:** ^{64}Cu-DOTA-alendronate is a promising PET imaging agent for the sensitive and specific detection of mammary tumors as well as the differentiation of malignant versus benign tumors based on absolute labeling uptake.

Key Words: ^{64}Cu-DOTA-alendronate; bisphosphonate; microcalcification; breast cancer; rat

J Nucl Med 2017; 58:1373–1379
DOI: 10.2967/jnumed.117.190850

Breast cancer is the most common invasive cancer in women worldwide (*1*). Early detection is paramount in improving chances of remission and survival by allowing treatment before the cancer can progress or metastasize. Currently, the most widely used form of breast cancer screening is mammography, which uses low-energy radiography to visualize the microarchitecture of the breast to detect masses or microcalcifications, which may indicate cancer (*2*). Although mammography remains the preferred screening modality for breast cancer in the general population (*3*), over the last decade controversy has grown surrounding the use of mammograms. Numerous studies indicate that while mammography detects some cancers that would otherwise go unnoticed for periods of time, the resulting overall decrease in mortality rates of women is minuscule (*4*). Because of a discouragingly high false-positive rate, mammograms cause considerable stress and lead to a high number of unnecessary, invasive biopsies, with only 10%–40% actually demonstrating cancer (*3*).

The principal aspect of a mammogram used to interpret areas of potential cancer is the presence of microcalcifications (*5*). There are many types of microcalcifications found in breast tissue. They can be composed of varying combinations and concentrations of oxalate and phosphate with calcium magnesium, sodium, potassium, iron, and zinc ions (*6*); however, mammograms can detect only certain types that are sufficiently dense to be seen on radiography. The most common type of microcalcification in normal tissue and benign lesions is calcium oxalate, and the most common type in malignant lesions is hydroxyapatite (*1,7,8*). Recent studies show that the size, shape, distribution, and most of all composition of microcalcifications are significantly correlated with tumor type (*8–10*). In this study, we sought to exploit this observation using a bisphosphonate, which has a high affinity for hydroxyapatite and other calcium crystals (*11*), including those not visible by mammography, as a sensitive targeting agent for these microcalcifications. The ability to predict microcalcification type before biopsy would significantly increase the specificity and utility of breast cancer screening.

Bisphosphonates are a class of drugs typically prescribed to prevent the loss of bone mass in diseases such as osteoporosis. Over the past 5 y, clinicians have observed that women taking bisphosphonates have improved breast cancer survival rates and chemotherapy efficacy (*12,13*). As a result, many clinicians now administer bisphosphonates to supplement chemotherapy regimens

Received Jan. 26, 2017; revision accepted Apr. 11, 2017.
*For correspondence or reprints contact: John E. Shively, Department of Molecular Immunology, Beckman Research Institute of the City of Hope, 1450 E. Duarte Rd., Duarte, CA 91010.
E-mail: jshively@coh.org
Published online Apr. 27, 2017.

(*13*). Although bisphosphonates have been minimally investigated as bone-targeting agents for PET imaging of bone disease, they have not been investigated as human breast cancer PET imaging agents (*14*).

Although current established PET imaging agents such as ^{18}F-FDG and ^{18}F-NaF are effective for detection of many cancer types (including breast cancer metastases), they are not effective in detecting primary breast cancer. ^{18}F-FDG is not sufficiently sensitive to distinguish small, in situ malignancies (*15*), and ^{18}F-NaF indirectly visualizes bony tumors with bone reaction–dependent uptake and is thus not effective at labeling nonactive, soft-tissue structures such as calcifications in breast tumors (*16*). This lack of efficacy in established PET imaging agents further reinforces the need for an effective breast cancer PET imaging agent.

Although several bisphosphonates are used clinically to treat osteoporosis, we chose alendronate for this study because of its accessible amino group suitable for conjugation chemistry and its relatively high affinity for calcium phosphate crystals compared with other bisphosphonates (*17*). The commonly used and clinically relevant chelating agent DOTA was chosen because we have used it extensively and successfully to radiolabel DOTA antibodies with ^{64}Cu for translational clinical trials (*18,19*). Radioisotopes for PET imaging are typically selected on the basis of the half-life of the carrier molecule. However, with alendronate having a 12-y half-life (*20*), ^{64}Cu was chosen because of its intermediate half-life of 12.7 h, which permits PET scans up to 48 h after injection while still maintaining acceptable dosimetry to the patient. This collectively led to our selection of ^{64}Cu-DOTA-alendronate as our PET imaging agent.

One of the major hurdles to the improvement of breast cancer imaging has been the lack of appropriate animal models that accurately recapitulate both the normal and the pathologic conditions seen in human breast tissue. Female rats have 6 pairs of mammary glands, with 2 of these pairs (thoracic and abdominal) being large and discrete. In contrast to mice, with an adult size of 300–500 g, rats are large enough for structures, such as microcalcifications, to be differentiated by PET within a mammary gland. It has been reported that aging rats develop microcalcifications in their mammary glands (*21*) and, more recently, that they can even be implanted with, or stimulated to grow, mammary calcifications (*22*). Here, we report the use of aged, female, retired breeder Sprague–Dawley rats as models for both normal and pathologic human breast tissue microcalcifications without any artificial microcalcification growth induction. Normal and benign tumor conditions were created without any experimental manipulation, and malignant tumors were induced with the carcinogen *N*-nitroso-*N*-methylurea, which reliably produces mammary carcinomas in rats.

Using the calcification binding properties of alendronate, and our rat model of human breast cancer, we synthesized DOTA-alendronate and administered ^{64}Cu-DOTA-alendronate (Fig. 1) to normal or tumor-bearing aged, female, retired breeder Sprague–Dawley rats for PET imaging. We subsequently imaged mammary tissues with light, confocal, and electron microscopy to verify the microcalcification-targeting specificity of DOTA-alendronate. Tumor uptake, biodistribution, and dosimetry studies were also performed to evaluate the efficacy and safety of ^{64}Cu-DOTA-alendronate with the goal of developing ^{64}Cu-DOTA-alendronate for the detection and noninvasive differentiation of malignant versus benign breast tumors with PET.

MATERIALS AND METHODS

Animal Models

Female, retired breeder (minimum, 5 litters) Sprague–Dawley rats (250–500 g; age, 12–18 mo) (Charles River Laboratories) were used and pair-housed in individually ventilated cages under standard conditions. Ten aged, retired breeder female rats received a single 50 mg/kg intraperitoneal injection of NMU (*N*-nitroso-*N*-methylurea) to produce intraductal carcinomas (*23*), which took approximately 3–9 mo to form. Twenty rats were allowed to age until they developed spontaneous fibroadenomas, and 14 of the 20 rats developed fibroadenomas over a period of 1 y. Thirty rats were used for tumor-free controls and comparative dosimetry. All animal procedures were performed and conducted in an Association for Assessment and Accreditation of Laboratory Animal Care International–accredited, specific pathogen-free facility in accordance with Institutional Animal Care and Use Committee–approved procedures and the *Guide for the Care and Use of Laboratory Animals* (*24*).

Radiolabeling

DOTA-alendronate was dissolved in 0.1 M ammonium acetate, pH 7.0, and incubated with ^{64}Cu at a ratio of 37 MBq per μg of DOTA-alendronate (2.3×10^{10} MBq/mol; total of 74 MBq; volume, 200 μL) for 30 min at 43°C, then chased with an excess of 1 mM diethylenetriamine pentaacetic acid and incubated at room temperature for 15 min. Radiolabeling efficiency was more than 98% by instant thin-layer chromatography with a 0.9% NaCl running buffer. Doses (37–74 MBq per rat) were diluted to 200 μL with 1% human serum albumin in saline.

PET Imaging

PET scans were acquired with an Inveon microPET/CT scanner (Siemens Medical Solutions). For dynamic PET scans, rats were anesthetized with 2%–4% isoflurane in oxygen, urinary catheterized, placed on the PET scanner, and injected with a single intravenous dose of 1 μg of ^{64}Cu-DOTA-alendronate per 250 g of body weight radiolabeled at 37 MBq/μg DOTA-alendronate (2.3×10^{10} MBq/mol) in 1% human serum albumin–buffered saline through a tail vein catheter. For the blocking study, the rat received 100 μg of nonradiolabeled DOTA-alendronate 1 h before a 1-μg imaging dose at 37 MBq/μg.

Biodistribution and Dosimetry

Rats were humanely euthanized at various time points for each experiment (immediately after a PET scan). Tissues were individually weighed, and then radioactivity was measured using an automated γ-counter (Wallac Wizard 3; Perkin Elmer) along with 3 dose standards. For dosimetric experiments and analysis, 8 rats were used to collect a total of 34 PET images over 48 h (Supplemental Table 1; supplemental materials are available at http://jnm.snmjournals.org). The projected human dose for an adult female was computed using OLINDA software (version 1.1, OLINDA/EXM; Vanderbilt University) with the rat ^{64}Cu-DOTA-alendronate pharmacokinetic data as input.

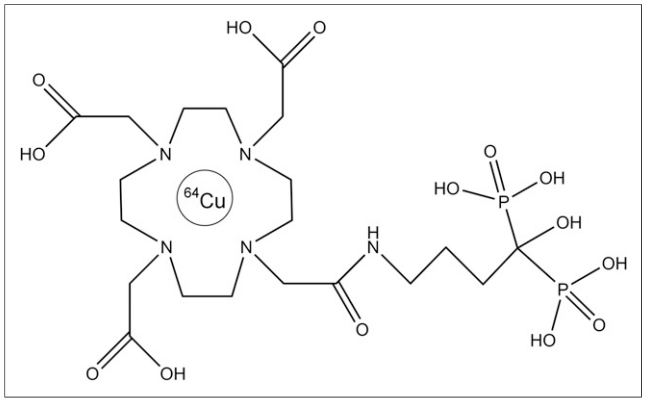

FIGURE 1. Chemical structure of ^{64}Cu-DOTA-alendronate.

RESULTS

Histology

The normal mammary gland histology of young versus aged retired breeder female rats is shown in Figure 2. Young rats showed few, if any, microcalcifications within their mammary glands; however, aged, retired breeder rats showed large, discrete, calcified crystals (microcalcifications) within the mammary ducts. With similar histology, morphology, local distribution, along with the presence of microcalcifications, the mammary glands in these rats are a morphologically similar recapitulation of human female breast tissue.

Rat Tumor PET Imaging

Whole-body PET images were obtained for ^{64}Cu-DOTA-alendronate in normal, benign tumor–bearing, and malignant tumor–bearing aged female retired breeder rats. Representative whole-body PET images used for our region-of-interest calculations for normal, benign, and malignant conditions are shown in Figure 3. Uptake of ^{64}Cu-DOTA-alendronate was observed in all 3 types of mammary tissue. At 1 h after injection, the average region-of-interest SUV of normal breast tissue was 0.30 (0.074 percentage injected dose per gram [%ID/g]) (n = 18), benign fibroadenoma was 0.74 (0.18 %ID/g) (n = 6), and malignant carcinoma was 2.0 (0.50 %ID/g), with tumor foci reaching 4.4 (1.1 %ID/g) (n = 4). The blood SUV at 1 h after injection was between 0.6 and 0.8 (0.15–0.20 %ID/g).

To further test in vivo binding specificity, we performed a blocking study of ^{64}Cu-DOTA-alendronate by preadministering a 100-fold excess (100 μg) of nonradiolabeled DOTA-alendronate 1 h before a 1-μg imaging dose of ^{64}Cu-DOTA-alendronate labeled at 37 MBq/μg (Fig. 4). This was done by imaging a rat with ^{64}Cu-DOTA-alendronate and then using the same rat 7 d later for the blocking experiment with unlabeled DOTA-alendronate. Another rat received 2 equivalent doses of ^{64}Cu-DOTA-alendronate, 1 wk apart, as a control to ensure that repeated administration itself did not affect binding levels 1 wk later (data not shown). Repeated administration 1 wk apart did not significantly affect mammary gland concentration; however, blocking with unlabeled DOTA-alendronate resulted in a 39% decrease in the SUV of mammary tissue (0.65 to 0.39).

Confocal and Electron Microscopy of Microcalcifications

Fluorescent Confocal Microscopy. Fluorescent confocal microscopy was performed on tissues collected from normal and tumor-bearing rats after PET imaging and tissue biodistribution. Representative images from 4 different physiologic and pathologic states of mammary tissue are shown in Figure 5. Mammary tissue from tumor-free, aged, retired breeder rats contained numerous, discrete, crystal-like structures stained specifically with FAM (carboxyfluorescein)-alendronate within the lumen of mammary ducts. Amorphous, nonspecific material was present within the ductal lumens of benign tumors, which were also positive for FAM-alendronate, 4′,6-diamidino-2-phenylindole, and wheat germ agglutinin-Alexa555. Calcifications were also visible within the lumen and between the glands of malignant carcinomas. The material within the ductal lumen was nonspecifically stained and similar to that seen in benign tumors; however, FAM-alendronate was highly specific to the small intercellular and intracellular crystalline structures with negligible background and nontarget staining. Kidneys containing nephroliths from the same rats were also stained as a positive control to validate the sensitivity and specificity of alendronate for calcium crystals. Individual, nonmerged confocal images are shown in Supplemental Figure 1.

Electron Microscopy and EDX (Energy-Dispersive X-Ray) Elemental Analysis. Tissue samples from normal rat mammary tissue and rats with benign or malignant tumors that were imaged with ^{64}Cu-DOTA-alendronate were prepared and processed for serial block face scanning electron microscopy. Two- and 3-dimensional scanning electron microscopy images revealed osmiophilic structures consistent with microcalcifications within the mammary ductal lumens of normal rats and in benign tumors. In malignant tumors, these structures were located within and between mammary gland cells (Fig. 6). The Amira 3D reconstruction software showed a diffuse distribution of these structures throughout the neoplastic mammary tissue (Supplemental Video 1). These results are consistent with our confocal microscopy observations. EDX analysis of microcalcifications (Supplemental Figure 2) revealed that these microcalcifications were devoid of carbon and contained high concentrations of calcium and oxygen.

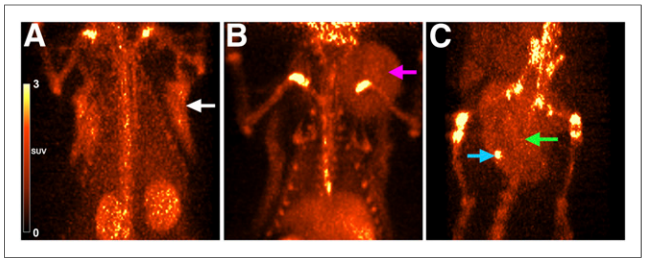

FIGURE 3. Representative PET images of normal and tumor-bearing aged, retired breeding rats 1 h after injection with ^{64}Cu-DOTA-alendronate. (A) Normal mammary gland (white arrow) (SUV, 0.3). (B) Mammary fibroadenoma (pink arrow) (SUV, 0.74). (C) Mammary carcinoma (green arrow) (SUV, 2.0) with intense calcification foci (blue arrow) (SUV, 4.4).

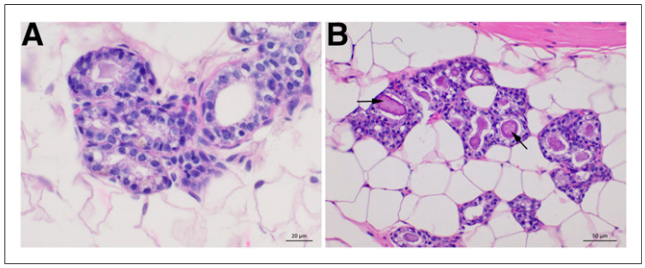

FIGURE 2. Hematoxylin and eosin histology of female Sprague–Dawley rat mammary tissues of 6-mo-old rat (A) and 18-mo-old retired breeder rat with large, defined mammary microcalcifications (B).

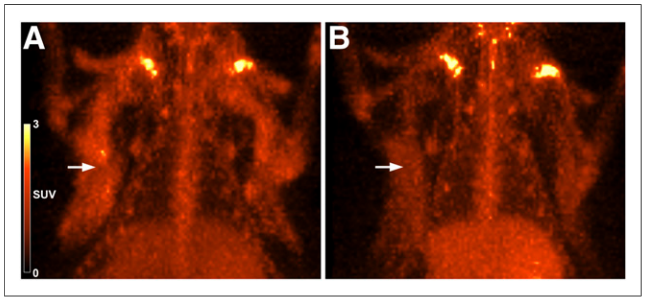

FIGURE 4. ^{64}Cu-DOTA-alendronate specificity in rat mammary glands. (A) PET image (1 h after injection) of normal mammary tissue uptake of ^{64}Cu-DOTA-alendronate (SUV, 0.65). (B) PET image (1 h after injection) of same rat 1 wk later, with preadministration of nonradiolabeled DOTA-alendronate 1 h before dosing with ^{64}Cu-DOTA-alendronate (SUV, 0.39).

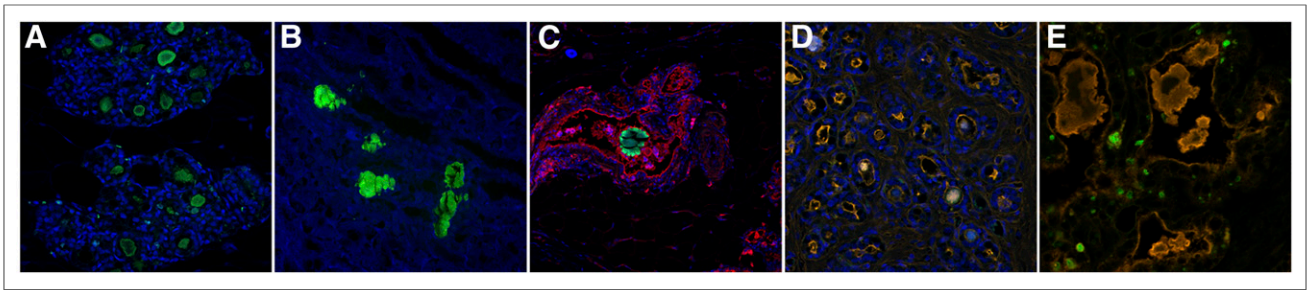

FIGURE 5. Fluorescent confocal microscopy images of mammary glands in aged, retired breeder Sprague–Dawley rats demonstrating differences in microcalcification characteristics under normal and neoplastic conditions. Tissues were stained with FAM-alendronate (green), WGA-Alexa555 (red), and DAPI (blue). (A) Normal, aged retired breeder rat. (B) Rat kidney nephroliths (positive control). (C) Lactating rat. (D) Benign fibroadenoma. (E) Malignant adenocarcinoma.

Biodistribution and Dosimetry of ^{64}Cu-DOTA-Alendronate in Normal Rats

The biodistribution of ^{64}Cu-DOTA-alendronate in aged, female, retired breeder Sprague–Dawley rats is presented in Table 1 as the %ID/g and percentage injected dose per organ of all major tissues over 48 h. All values are decay-corrected to show the biologic activity and pharmacokinetics of the drug. The 4 primary organs of concern (kidney, bone, blood, and liver) were also measured by region-of-interest tracing of PET images at 34 time points for each organ (Supplemental Table 1). Figure 7 is a graphical reflection of the pharmacokinetics of ^{64}Cu-DOTA-alendronate in the 4 highest-concentration tissues, demonstrating the trends over the first hour and over the next 48 h.

Blood, kidney, and urinary bladder levels peaked within the first few minutes and then sharply fell as the drug was excreted through the kidneys and voided from the bladder. At 1 h after injection, the bladder, kidneys, and stifle joint had the highest activity levels. Renal uptake was high and partially due to the known route of excretion of bisphosphonates (*17*), but also due to nephroliths, which are generally present and numerous in rats of this age (*25*). By 4 h, the clearance of ^{64}Cu-DOTA-alendronate through the kidneys and into the urine was complete and bladder activity was undetectable after voiding. However, the kidneys and stifle joints maintained elevated organ activity levels. All organ activity plateaued by 4 h after injection and gradually decreased over the next 48 h, with the exception of the liver, which gradually increased over 48 h.

Using OLINDA/EXM, we calculated the relative dose of ^{64}Cu-DOTA-alendronate for each organ of an adult, female human assuming similar pharmacokinetics between humans and rats (Table 2). The organs with the highest estimated dose were the large intestine (due to its adjacency to the bladder) and the kidneys (through which the drug is excreted). The organs with the lowest estimated doses were the upper abdominal and thoracic organs (lungs, spleen, thymus, and thyroid). The estimated total effective dose for an adult woman is 0.0418 mSv/MBq.

DISCUSSION

Our use of aged, retired breeder, female rats as ideal models for evaluating breast cancer imaging techniques, especially those that involve microcalcifications, allowed us to study the potential for ^{64}Cu-DOTA-alendronate in a natural, nonartificially induced model, which accurately recapitulated the physiologic characteristics of human breasts. These rats underwent multiple cycles of pregnancy and parturition-associated hypertrophy and hyperplasia of mammary glands with subsequent atrophy after weaning. This simulates normal human pregnancy and the associated changes in breast physiology. These rats also age rapidly and undergo menopause similar to women (*26*). Therefore, throughout their lives, these rats underwent many of the same physiologic events as human women. Our findings that their mammary tissues, including discrete microcalcifications, are similar to those seen in humans indicate that aged, retired breeder, female rats are a useful model for evaluating breast imaging techniques.

Radiolabeling of DOTA-alendronate with ^{64}Cu was greater than 98% by instant thin-layer chromatography at several specific activities, up to 37 MBq per μg of DOTA-alendronate. The images in Figure 3 demonstrate excellent specificity for microcalcifications within mammary tissue with minimal background uptake. Though the mammary gland has a lower level of ^{64}Cu-DOTA-alendronate accumulation on a per gram basis than other organs such as kidney, bone, liver, and bladder, this drug is intended as an imaging agent, not a targeted therapy agent. Therefore, as long as the off-target levels are within a safe threshold, the most important characteristics of the drug are that it reaches the desired organ (here, the microstructures within the organ) and has low background labeling of

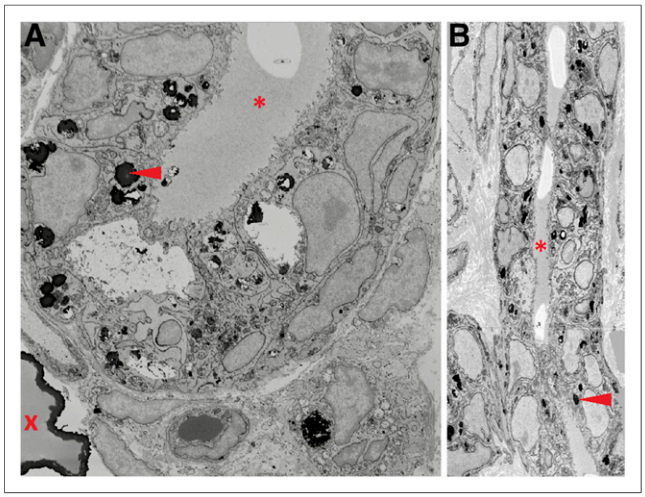

FIGURE 6. Serial block face scanning electron microscopy (SBEM) of mammary duct from malignant carcinoma in aged retired breeder rat. Transverse (A) and longitudinal (B) views of SBEM image stack demonstrating large microcalcification (red X) and smaller, osmiophilic structures (red arrowheads) within or between mammary luminal and myoepithelial cells but not within ductal lumen (red asterisk). Images were taken at 18,500× magnification.

TABLE 1
Pharmacokinetics of ^{64}Cu-DOTA-Alendronate in Normal Female Rats Over 48 Hours

	Time (h)															
	%ID/g*								%ID/organ*							
Organ	1.79	4.62	14.4	15.1	26.2	29.3	41.7	48.6	1.79	4.62	14.4	15.1	26.2	29.3	41.7	48.6
Blood†	0.15	0.24	0.17	0.15	0.22	0.25	0.17	0.17	1.97	3.33	2.26	1.96	2.80	3.53	2.44	2.50
Kidneys†	1.29	1.25	0.82	0.99	0.98	0.89	0.71	0.83	2.04	2.16	1.57	2.16	1.92	1.87	1.40	1.67
Liver†	0.27	0.26	0.36	0.35	0.53	0.52	0.49	0.52	1.71	2.34	2.79	3.08	4.27	4.61	4.57	4.86
Femur†	1.54	1.54	1.61	1.37	1.62	1.36	1.67	1.56	1.00	1.34	1.55	1.40	1.52	1.51	1.68	1.87
Knee joint†	1.69	1.87	2.35	2.27	2.06	1.81	2.25	2.12	1.22	1.56	1.73	1.63	1.91	2.05	2.13	2.42
Heart	0.10	0.16	0.14	0.14	0.18	0.20	0.18	0.17	0.07	0.13	0.13	0.15	0.16	0.20	0.15	0.20
Lung	0.12	0.19	0.14	0.14	0.19	0.20	0.17	0.18	0.10	0.30	0.15	0.14	0.19	0.22	0.16	0.16
Spleen	0.06	0.13	0.12	0.12	0.17	0.19	0.15	0.15	0.02	0.06	0.06	0.06	0.07	0.09	0.06	0.07
Pancreas	0.10	0.18	0.10	0.08	0.16	0.15	0.10	0.11	0.17	0.32	0.19	0.16	0.24	0.33	0.21	0.20
Stomach‡	0.08	0.23	0.11	0.06	0.11	0.09	0.02	0.05	0.28	0.46	0.49	0.23	0.40	0.36	0.21	0.39
Small intestine‡	0.17	0.38	0.26	0.25	0.33	0.29	0.26	0.23	1.20	2.44	2.08	2.28	2.06	2.67	1.70	1.93
Large intestine‡	0.07	0.30	0.49	0.37	0.47	0.44	0.26	0.25	0.41	1.87	3.91	2.27	3.76	3.69	2.80	2.33
Muscle	0.07	0.04	0.03	0.07	0.05	0.06	0.05	0.05	0.04	0.04	0.04	0.07	0.06	0.06	0.06	0.07
Mammary			0.10	0.10	0.11	0.10	0.12	0.11			0.01	0.02	0.01	0.01	0.01	0.01
Vertebrae	0.93	0.96	0.81	1.22	1.12	0.95	1.02	1.12	0.81	1.06	1.11	0.97	0.95	1.07	1.03	1.08
Bladder	2.59		0.11	0.04	0.05	0.04	0.03	0.02	2.06		0.05	0.01	0.01	0.02	0.03	0.02
Red marrow¶	0.05	0.07	0.05	0.05	0.07	0.08	0.05	0.05	0.13	0.22	0.15	0.13	0.19	0.23	0.16	0.17

*Values were obtained from individual tissue γ-counts.
†Primary organs of concern were also measured by volume-of-interest tracing of PET images at 34 time points for each organ (Supplemental Table 1).
‡Includes contents.
¶Calculated assuming red marrow–to–blood activity concentration ratio of 0.31; red marrow total volume–to–blood total volume ratio of 0.21, rat blood volume of 64 mL/kg.

adjacent tissues (here, mammary glands and ducts). The blocking experiment shown in Figure 4 suggests that the use of higher specific activity may increase relative mammary tissue uptake and further reinforces the specificity of ^{64}Cu-DOTA-alendronate for mammary microcalcifications.

^{64}Cu-DOTA-alendronate effectively targets mammary tissue and has the potential to be a contrast agent for human breast PET imaging. PET images showed excellent contrast between mammary microcalcifications and surrounding soft tissue. This allowed the visualization of individual large microcalcifications as well as clusters of small microcalcifications. The predictive value of this agent lies in the observation that benign tumors have a 2- to 3-fold increase in ^{64}Cu-DOTA-alendronate accumulation and that malignant tumors have a roughly 7- to 15-fold increase over that of normal tissue. In vitro analysis of mammary tissue with FAM-alendronate demonstrates the specificity of microcalcification binding using other alendronate derivatives. These experiments supported our hypothesis that the targeting of this agent in mammary tissue was due, almost entirely, to its specific binding to calcified structures, and not due to nonspecific soft-tissue uptake.

In this study, we observed that different tumor types had significantly different ^{64}Cu-DOTA-alendronate uptake, and these variations in uptake (and resultant PET image intensity) were inversely proportional to the radiopacity of these tumor types on traditional mammograms (*27,28*). This finding indicates that the disparities in observed PET image intensity are due to the differential binding of ^{64}Cu-DOTA-alendronate to the different types of calcifications present in these different mammary tumors. However, further studies are needed to determine whether the differences in ^{64}Cu-DOTA-alendronate binding are due to quantity, composition, or density of the microcalcifications in these different tissue types. This observation reinforces the potential utility of this agent to be used in concert with, or as a follow-up to, mammography to further aid in tumor differentiation based on the relationship between labeling intensity and mammogram radiopacity.

As visible by hematoxylin and eosin and confocal histology, our rat mammary glands showed characteristics similar to their equivalent tissues in humans with normal mammary gland, demonstrating occasional variable-sized solid crystals; benign tumors showing numerous, large, poorly defined crystals; and malignant carcinomas having small, intracellular, and intercellular calcifications. This is further supported by electron microscopy, which shows the spatial distribution of these microcalcifications within and between the ductal cells in a mammary duct in a carcinoma. These small calcifications are indicative of malignancy and are difficult to see with traditional hematoxylin and eosin; thus, fluorescent FAM-alendronate may be useful for histopathologic analysis of biopsy sections to more accurately evaluate size, distribution, and even composition of microcalcifications. As seen in Figure 5,

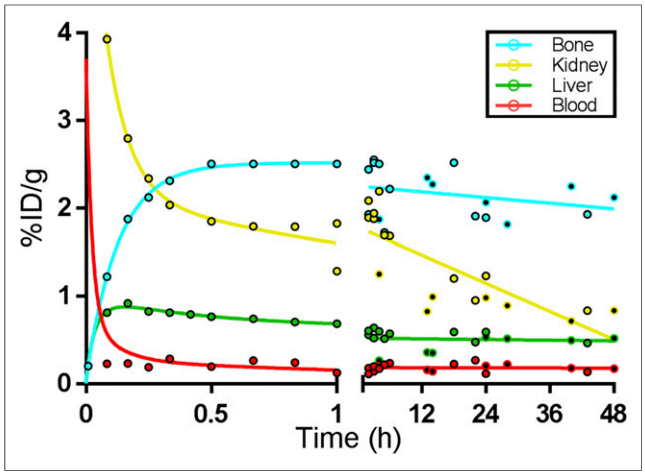

FIGURE 7. Pharmacokinetics of ^{64}Cu-DOTA-alendronate in high-activity organs demonstrating trends over first hour and after 47 h. Uptake was determined by tissue γ-counting (filled circles) or by ROI measurements from PET images (open circles). Data are corrected for radioactive decay.

FAM-alendronate is highly specific for microcalcifications with little to no background fluorescence.

Serial block face scanning electron microscopy of microcalcifications offers an interesting adjunct pathologic tool to observe the spatial distribution of microcalcifications within a tumor and use that distribution to aid in diagnosis. As this new technology is used more, we may start to use it to aid in the diagnosis of certain cancers based on the 3-dimensional orientation of cells and structures in different types of cancers.

Previous studies have shown that unconjugated alendronate, like other bisphosphonates, is rapidly cleared from the blood (95% in 6 h) and distributed to all major organs. Over the first 72 h after administration, alendronate steadily dissociates from noncalcified tissues and is excreted unchanged in the urine. After 72 h, approximately 50% of the initial dose is bound to bone where it has a terminal half-life of 12 y (*20*). The biodistribution and pharmacokinetics of ^{64}Cu-DOTA-alendronate in this study were consistent with these published standards for unconjugated alendronate and showed decreasing soft-tissue concentration and stable or increasing bone concentration over the first 72 h. Taken in conjunction with our finding that more than 95% of ^{64}Cu remains bound to DOTA-alendronate after 48 h in serum (Supplemental Fig. 1), the addition of DOTA and ^{64}Cu does not seem to have significantly affected the pharmacokinetics of alendronate. One exception to the predicted pharmacodynamics was the observation that liver values gradually rose over 48 h instead of falling like other tissues. This is likely due, in part, to metabolism of ^{64}Cu-DOTA-alendronate both in the liver itself and in other organs. Once liberated from DOTA, free copper primarily binds to albumin in the blood and is transported into hepatocytes where it is sequestered (*29*).

Typical comparative dosimetric analyses use 3–6 animals per time point for 3–7 time points. This equates to between 9 and 42 data points. In the standardized dosimetry trial alone, we used 8 animals to collect between 27 and 36 values (depending on organ) for more than 15 different time points. Analysis of dosimetry and biodistribution values in rats with OLINDA/EXM taking careful, conservative considerations for every organ and detailed calculations for urinary clearance and bone marrow predicts a total effective human dose per unit injected activity of 0.0418 mSv/MBq. With an injected dose of 370 MBq, the resulting human dose for a PET examination would be 15.5 mSV. This dose is within the acceptable range for clinical PET imaging agents and furthers the potential for translation into human patients.

TABLE 2
Estimated Radiation Doses for ^{64}Cu-DOTA-Alendronate

Organ	Equivalent dose per unit injected dose activity (mSv/MBq)
Adrenals	2.00E−02
Brain	1.61E−02
Breasts	4.22E−03
Gallbladder wall	2.26E−02
Lower large intestine wall	1.59E−01
Small intestine	6.11E−02
Stomach wall	3.03E−02
Upper large intestine wall	1.13E−01
Heart wall	6.36E−02
Kidneys	1.08E−01
Liver	4.63E−02
Lungs	9.61E−03
Muscle	6.89E−03
Ovaries	2.56E−02
Pancreas	4.75E−02
Red marrow	1.55E−02
Osteogenic cells	4.56E−02
Skin	1.38E−02
Spleen	1.35E−02
Thymus	1.77E−02
Thyroid	1.52E−02
Urinary bladder wall	9.94E−02
Uterus	2.30E−02
Total body	2.01E−02
Total effective dose	4.18E−02

CONCLUSION

This research has effectively addressed the 2 major obstacles to the advancement of breast cancer screening: the lack of specificity in imaging modalities and the absence of effective small-animal models to test them. We have demonstrated a compelling use for alendronate as a PET imaging agent (in the form of ^{64}Cu-DOTA-alendronate) for the detection and noninvasive differentiation of malignant and benign mammary tumors. We also present the aged, retired breeder, female Sprague–Dawley rat as an effective animal model that is uniquely suited for use in breast cancer imaging research. We have likewise shown the utility of FAM-alendronate as a contrast agent for histologic detection of calcium crystals in tissues by confocal microscopy. Our collective evidence including PET imaging, dosimetry, biodistribution, and confocal and electron microscopy suggests that ^{64}Cu-DOTA-alendronate could be developed into a safe and powerful imaging agent for the detection and the noninvasive diagnosis of human breast tumors containing microcalcifications.

DISCLOSURE

Research reported in this publication was supported by the National Cancer Institute of the National Institutes of Health under award number P30CA033572. No other potential conflict of interest relevant to this article was reported.

ACKNOWLEDGMENTS

Desiree Lasiewski assisted with PET imaging. Richard Ermel and Trinka Adamson provided animal resources. Joan Mortimer collaborated for translational processing. Paul Yazaki assisted with conjugations. Ricardo Zerda and Zhuo Li prepared samples and images for electron microscopy. Brian Armstrong assisted with preparation and imaging for confocal microscopy.

REFERENCES

1. Reeder JG, Vogel VG. Breast cancer prevention. *Cancer Treat Res.* 2008;141: 149–164.
2. Gøtzsche PC, Nielsen M. Screening for breast cancer with mammography. *Cochrane Database Syst Rev.* 2011;CD001877.
3. Siu AL, Force USPST. Screening for breast cancer: U.S. Preventive Services Task Force recommendation statement. *Ann Intern Med.* 2016;164:279–296.
4. Croswell JM, Kramer BS, Kreimer AR, et al. Cumulative incidence of false-positive results in repeated, multimodal cancer screening. *Ann Fam Med.* 2009; 7:212–222.
5. Tse GM, Tan PH, Pang AL, Tang AP, Cheung HS. Calcification in breast lesions: pathologists' perspective. *J Clin Pathol.* 2008;61:145–151.
6. Scott R, Kendall C, Stone N, Rogers K. Elemental vs. phase composition of breast calcifications. *Sci Rep.* 2017;7:136.
7. Saslow D, Hannan J, Osuch J, et al. Clinical breast examination: practical recommendations for optimizing performance and reporting. *CA Cancer J Clin.* 2004;54:327–344.
8. Scimeca M, Giannini E, Antonacci C, Pistolese CA, Spagnoli LG, Bonanno E. Microcalcifications in breast cancer: an active phenomenon mediated by epithelial cells with mesenchymal characteristics. *BMC Cancer.* 2014;14:286.
9. Baker R, Rogers KD, Shepherd N, Stone N. New relationships between breast microcalcifications and cancer. *Br J Cancer.* 2010;103:1034–1039.
10. Fandos-Morera A, Prats-Esteve M, Tura-Soteras JM, Traveria-Cros A. Breast tumors: composition of microcalcifications. *Radiology.* 1988;169:325–327.
11. Bhushan KR, Tanaka E, Frangioni JV. Synthesis of conjugatable bisphosphonates for molecular imaging of large animals. *Angew Chem Int Ed Engl.* 2007;46:7969–7971.
12. Zhu J, Zheng Y, Zhou Z. Oral adjuvant clodronate therapy could improve overall survival in early breast cancer: results from an updated systematic review and meta-analysis. *Eur J Cancer.* 2013;49:2086–2092.
13. Ben-Aharon I, Vidal L, Rizel S, et al. Bisphosphonates in the adjuvant setting of breast cancer therapy–effect on survival: a systematic review and meta-analysis. *PLoS One.* 2013;8:e70044.
14. Ogawa K, Takai K, Kanbara H, et al. Preparation and evaluation of a radiogallium complex-conjugated bisphosphonate as a bone scintigraphy agent. *Nucl Med Biol.* 2011;38:631–636.
15. Kumar R, Chauhan A, Zhuang H, Chandra P, Schnall M, Alavi A. Clinicopathologic factors associated with false negative FDG-PET in primary breast cancer. *Breast Cancer Res Treat.* 2006;98:267–274.
16. Bastawrous S, Bhargava P, Behnia F, Djang DS, Haseley DR. Newer PET application with an old tracer: role of ^{18}F-NaF skeletal PET/CT in oncologic practice. *Radiographics.* 2014;34:1295–1316.
17. Russell RG. Bisphosphonates: mode of action and pharmacology. *Pediatrics.* 2007;119(suppl 2):S150–S162.
18. Mortimer JE, Bading JR, Colcher DM, et al. Functional imaging of human epidermal growth factor receptor 2-positive metastatic breast cancer using ^{64}Cu-DOTA-trastuzumab PET. *J Nucl Med.* 2014;55:23–29.
19. Li L, Bading J, Yazaki PJ, et al. A versatile bifunctional chelate for radiolabeling humanized anti-CEA antibody with In-111 and Cu-64 at either thiol or amino groups: PET imaging of CEA-positive tumors with whole antibodies. *Bioconjug Chem.* 2008;19:89–96.
20. Cocquyt V, Kline WF, Gertz BJ, et al. Pharmacokinetics of intravenous alendronate. *J Clin Pharmacol.* 1999;39:385–393.
21. Foster WG, Younglai EV, Boutross-Tadross O, Hughes CL, Wade MG. Mammary gland morphology in Sprague-Dawley rats following treatment with an organochlorine mixture in utero and neonatal genistein. *Toxicol Sci.* 2004;77:91–100.
22. Inoue K, Liu F, Hoppin J, et al. High-resolution computed tomography of single breast cancer microcalcifications in vivo. *Mol Imaging.* 2011;10:295–304.
23. Gullino PM, Pettigrew HM, Grantham FH. N-nitrosomethylurea as mammary gland carcinogen in rats. *J Natl Cancer Inst.* 1975;54:401–414.
24. National Research Council (U.S.). Committee for the Update of the Guide for the Care and Use of Laboratory Animals, Institute for Laboratory Animal Research (U.S.), National Academies Press (U.S.). *Guide for the Care and Use of Laboratory Animals.* 8th ed. Washington, D.C.: National Academies Press; 2011.
25. Paterson M. Urolithiasis in the Sprague–Dawley rat. *Lab Anim.* 1979;13:17–20.
26. Wu JM, Zelinski MB, Ingram DK, Ottinger MA. Ovarian aging and menopause: current theories, hypotheses, and research models. *Exp Biol Med (Maywood).* 2005;230:818–828.
27. Radi MJ. Calcium oxalate crystals in breast biopsies: an overlooked form of microcalcification associated with benign breast disease. *Arch Pathol Lab Med.* 1989;113:1367–1369.
28. Tornos C, Silva E, el-Naggar A, Pritzker KP. Calcium oxalate crystals in breast biopsies: the missing microcalcifications. *Am J Surg Pathol.* 1990;14:961–968.
29. Cousins RJ. Absorption, transport, and hepatic metabolism of copper and zinc: special reference to metallothionein and ceruloplasmin. *Physiol Rev.* 1985;65:238–309.